APPLIED PHYSICS LETTERS **89**, 251909 (2006)

Structural evolution in TiCu-based bulk metallic glass with large compressive plasticity

G. Wang, Y. H. Liu, P. Yu, D. Q. Zhao, M. X. Pan, and W. H. Wang[a)]
Institute of Physics, Chinese Academy of Sciences, Beijing 100080, People's Republic of China

(Received 17 October 2006; accepted 16 November 2006; published online 19 December 2006)

The structural evolution during deformation is investigated in a work hardenable ductile TiCu-based bulk metallic glass by high-resolution electron microscopies. Two categories of crystalline morphologies, the scattered nanocrystallites and the nanocrystalline bands, are observed during the deformation. The nanocrystallization induced by deformation has implications for interpreting the unusual mechanical behavior of the glass. © *2006 American Institute of Physics*. [DOI: 10.1063/1.2423249]

The plastic deformation of bulk metallic glasses (BMGs) is highly localized to the narrow shear bands (SBs).[1–3] The strain and the thermal softening occurring in the SBs result in a very limited plastic strain ($<1.0\%$) and catastrophic failure,[4,5] which severely restrict the applications of BMGs. Recently, various ductile monolithic BMGs with a large strain value ($>5.0\%$) and even work hardening behavior were developed by carefully modifying the chemical compositions.[6–11] This progress has triggered a great interest in the plastic deformation mechanism in BMGs in which dislocation systems and grain structures are absent. However, the reasons resulting in these behaviors in BMGs remain mysterious.[7,9,11]

To understand the mechanism of the strain localization, two models have been proposed from the viewpoint of local structural change induced by shear flow stress[1,12,13] and local temperature rise.[3,4] It remains important to clarify the structural evolution in BMG and especially in SBs during deformation.[4,14] In this work, we develop a class of TiCu-based BMGs that exhibits a large plastic strain and pronounced work hardening. These BMGs provide a valuable model for studying structural evolution accompanying the plastic deformation. We use high-resolution electron microscopies to resolve structural change in a representative work hardenable ductile $(\mathrm{Ti}_{0.5}\mathrm{Cu}_{0.5})_{84}\mathrm{Ni}_7\mathrm{Hf}_5\mathrm{Zr}_3\mathrm{Si}_1$ BMG. We propose that the plasticity and work hardening of the glass are attributed to the nanocrystallization in the SBs during deformation.

Alloy ingots were prepared by arc melting a mixture of pure metal elements, followed by suction casting into Cu mold to form rodlike BMGs. High-resolution transmission electron microscopy (HRTEM) specimens were mechanically thinned and polished to be less than 20 μm in thickness. The specimen was then subjected to ion milling at an incident angle of 5° for less than 30 min to electron transparency by using a Gatan 691 precision ion polishing system with liquid nitrogen cooling. The HRTEM observation was conducted on a JEOL JEL-2010 operating at 200 kV. Fractography was observed by using Philips XL 30 scanning electron microscope (SEM). Compressive test specimens were 4 mm in height and 2 mm in diameter. Compressive tests were conducted using an Instron 5500R1186 with a strain rate of $2\times10^{-4}\ \mathrm{s}^{-1}$.

The TiCu-based BMGs with the nominal compositions of $(\mathrm{Ti}_{0.5}\mathrm{Cu}_{0.5})_{84}\mathrm{Ni}_7\mathrm{Hf}_z\mathrm{Zr}_y\mathrm{Si}_x$ ($x=0,1$, $y=0-4$, and $z=4-9$) are obtained. Figure 1 shows the transmission electron microscopy (TEM) results of a representative $(\mathrm{Ti}_{0.5}\mathrm{Cu}_{0.5})_{84}\mathrm{Ni}_7\mathrm{Hf}_5\mathrm{Zr}_3\mathrm{Si}_1$ BMG. The lower magnification TEM image [Fig. 1(a)] exhibits a homogeneous feature, and the corresponding selected area electron diffraction (SAED) pattern shows the faint and diffuse ring. All these characterize a glassy structure of the alloy. X-ray diffraction pattern (not shown here) and the HRTEM image in Fig. 1(b) (showing a mazelike pattern without any crystalline feature) further confirm the homogeneous glassy phase of the alloy.

The compressive nominal stress-strain (σ-ε) curve of the BMG is shown in Fig. 2. After yielding, the BMG shows stress increase with strain indicating a work hardening up to 14.2%. The yielding stress, fracture stress, and the elastic modulus are measured to be 1879 MPa, 2723 MPa, and 96 GPa, respectively. The true σ-ε curve in the inset clearly exhibits an increase of the flow stress after yielding, and the plastic deformation shows two distinct stages with different work hardening rates θ: $\theta/G=d\sigma/d\varepsilon$ (G is the shear

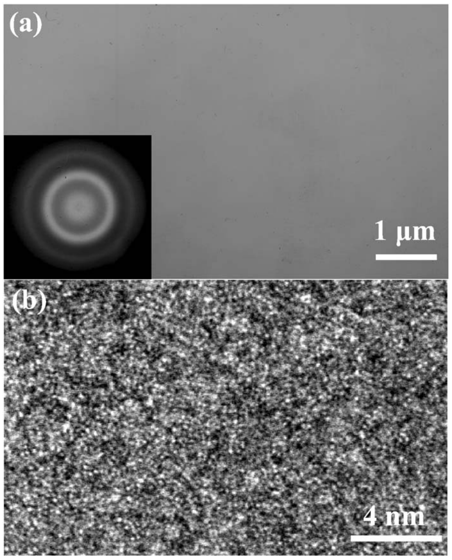

FIG. 1. Glassy features of the as-cast $(\mathrm{Ti}_{0.5}\mathrm{Cu}_{0.5})_{84}\mathrm{Ni}_7\mathrm{Hf}_5\mathrm{Zr}_3\mathrm{Si}_1$ BMG. (a) TEM bright field image plus SAED pattern. (b) HRTEM image.

[a)] Author to whom correspondence should be addressed; electronic mail: whw@aphy.iphy.ac.cn

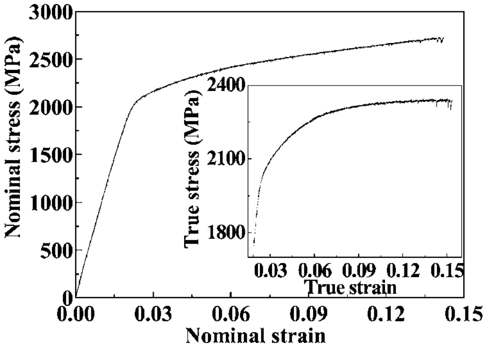

FIG. 2. Compressive nominal stress-strain behavior of the $(Ti_{0.5}Cu_{0.5})_{84}Ni_7Hf_5Zr_3Si_1$ BMG. The inset shows the corresponding true stress-strain curve.

modulus).[15] The values of θ/G in the first (total strain range of 2.0%–6.0%) and the second (6.0% to fracture) stages are 0.186 and 0.018, respectively. Three specimens, which were compressed to the total strains of 4.0% and 6.0% (corresponding to the first and the second deformation stages, respectively) and to fracture, were performed to investigate the SB evolution during the deformation.

The SEM observations of the surface of the specimens are exhibited in Fig. 3. The specimen subjected to the strain of 4.0% exhibits SBs with different orientations on its surface. The interactions of SBs are observed [Fig. 3(a)] while no SBs slip in this stage. For the specimen subjected to a strain of 6.0%, the SBs slip about 1.53 μm, as indicated in Fig. 3(b). For the fractured specimen, the slip distance of the SBs is promoted to ~4.54 μm [see Fig. 3(c)]. The shear fracture angle [the inset of Fig. 3(a)] is measured to be 49°, which is significantly higher than those of other BMGs with limited ductility.[16] The specimen shows a barrel shape due to the large plastic strain. The main morphologic feature of the fracture surface is veinlike patterns similar to those of other ductile BMGs.[7–10] Moreover, the smaller intershear band spacing and branched shear bands are observed on the surface of the fractured specimen, suggesting that more shear bands are activated during plastic deformation process [see Fig. 3(d)].

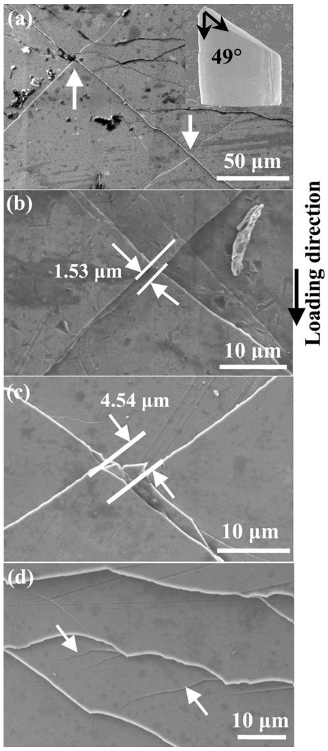

FIG. 3. SEM observations of the $(Ti_{0.5}Cu_{0.5})_{84}Ni_7Hf_5Zr_3Si_1$ BMG deformed with different strain values. (a) Deformed with a total strain of 4.0% (the inset is the side view of the fractured specimen). (b) Deformed with a total strain of 6.0%. (c) Deformed until fracture. (d) Highly branched SBs in the deformed BMG (as marked by arrows).

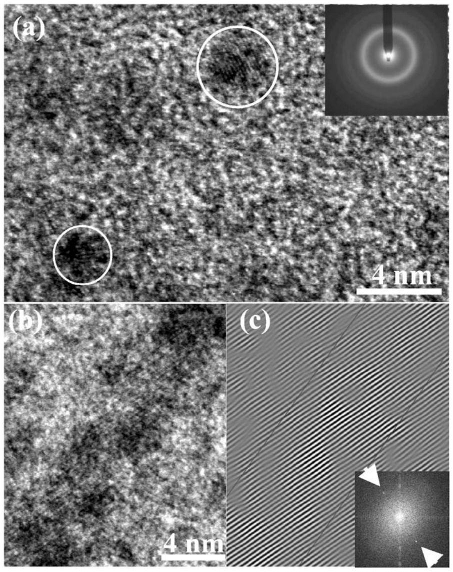

FIG. 4. HRTEM images for the $(Ti_{0.5}Cu_{0.5})_{84}Ni_7Hf_5Zr_3Si_1$ BMG deformed with a strain of 4.0%. (a) Microstructure of the scattered nanocrystallites. (b) Microstructure of the nanocrystalline band. (c) IFF image corresponding to the nanocrystalline band (inset is the FFT image).

The HRTEM image for the BMG (cut from the center of the sample where high density SBs are located) with 4.0% strain is shown in Fig. 4. The deformed BMG exhibits two categories of microstructural features: the nanoparticle and the nanocrystalline band. The nanoparticles with an average size of 4 nm are embedded in the glassy matrix and surround the SBs [Fig. 4(a)]. The SAED pattern of the nanoparticle region shows weak but sharp diffraction rings besides the typical amorphous diffraction ring [Fig. 4(a) inset]. This confirms the precipitation of nanoparticles in the glassy matrix. The unique nanoscale bands with an average width of ~6 nm can be observed in Fig. 4(b), which corresponds to the SB. In the band, the crystalline lattice fringes are clearly observed. The fast Fourier transformation (FFT) image [Fig. 4(c) inset] shows one pair of diffraction spots, indicating that the crystallite in the band has only one crystal plane. The inverse Fourier filtering (IFF) image corresponding to a pair of diffraction spots in the FFT image is shown in Fig. 4(c), in which the white dashes reflect the crystal plane. No grain boundary and misfit of the crystal plane are found.

The HRTEM observations close to the fracture surface in the fractured specimen also find the nanocrystallites and the nanocrystalline bands, while their sizes are obviously large. The scattered nanocrystallites have an average size of 8 nm [Fig. 5(a)]. The width of the band increases to ~21 nm [Fig. 5(b)]. The IFF image in Fig. 5(c), which corresponds to the pair of diffraction spots marked by arrows in the FFT image [the inset of Fig. 5(d)], shows a large number of dislocations in the band, and the crystalline plane misfits are along the shear direction.

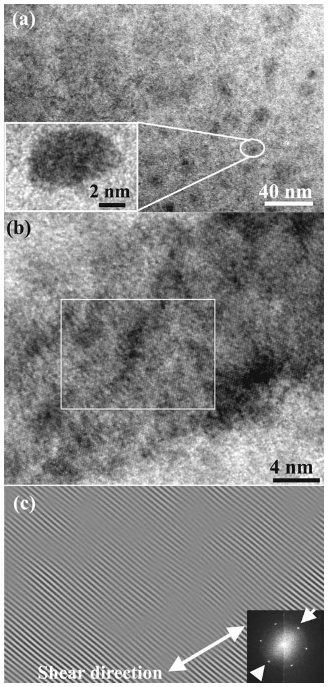

FIG. 5. HRTEM images for the fractured $(Ti_{0.5}Cu_{0.5})_{84}Ni_7Hf_5Zr_3Si_1$ BMG. (a) Structure of the scattered nanocrystallites. (b) Structure of the nanocrystalline band. (c) IFF image corresponding to the nanocrystalline band enclosed by a white rectangle frame in (b) (the inset is the FFT image).

Our observations suggest that the formation of the striplike crystallite in SBs is possibly due to the effect of both adiabatic heating and shear flow stress. The shear flow stress can result in a flow dilatation of amorphous materials well below glass transition temperature, enhance atomic mobility, and induce the crystallization.[12,13] The BMG subjected to 4.0% strain and total plastic deformations correspond to deformation times of ~260 and 790 s, respectively. Compared with the deformation duration (10 s) of nanoindentation induced nanocrystallization,[13] the large plastic deformation duration of the BMG is enough for the formation and growth of the striplike crystallite in SBs. The increase of the width of the band with increasing plastic strain indicates that the growth of the bands depends on the plastic deformation durations, which are different at different deformation stages.

Once the SB forms in the initial deformation stage, it starts to move driven by shear stress, and a remarkable temperature T rise is stimulated in SBs.[3,4] Because the heat-affected zone is about 200–1000 nm (Ref. 4) that is much wider than that of the SB (~20 nm), the momentary T increase induces the formation of the scattered nanocrystallites surrounding the SBs, and no nanocrystalline band structure is formed if the deformation duration is short enough, as the case in brittle BMGs. Therefore, although the nanocrystallization is activated by deformation in BMGs with limited ductility, it generates only isolated tiny nanocrystalline particles and does not influence the SB structure that is a layer of melted phase resulting from adiabatic heating. The strain softening leads to a sudden fracture of the BMGs with limited ductility. In the plastic BMGs, when large SBs slip develop, the shear flow stress and the frictional heating will further affect the SB and induce the formation of the nanocrystalline bands. Meanwhile, the nanoparticles with large size and high density are formed surrounding the SBs.

Our observations indicate that the deformation-induced structural evolution controls the deformation and work hardening in the BMG. In the initial deformation stage, because both sizes of the scattered nanocrystallites and the nanocrystalline bands are less than a critical size (11–18 nm)[17,18] of dislocation stability, the dislocation is impossibly stimulated in these nanocrystallites. The nanocrystalline bands and particles with a theoretical high shear strength[19] act as the reinforcing phase and significantly improve the strength of the BMG, and the growth of nanocrystallites and nanobands will further improve the strength with increasing plastic strain. Therefore, the stress-strain behavior exhibits the high work hardening rate in this stage. On the other hand, the nanocrystallites and the hardened SBs can induce the shear delocalization and crack blunt[20] and trigger the SB multiplication, thus yielding a global ductility.[8] This is confirmed by highly branched SBs and small intershear band spacing in the BMG observed by SEM.

When the size of the nanocrystalline bands is larger than the critical size, the dislocations in the crystalline bands can be activated. In this case, the motion of dislocation should be an important event in the nanocrystalline bands, and the shear deformation should be localized in the widened nanocrystalline bands. As a result, the shear avalanche manifesting a sudden failure after a small plastic strain at a macroscopic scale is prohibited.[5] The work hardening rate of 0.018 in the second stage is close to that of the Ti-based compound ($\theta/G \approx 0.011$),[15] which suggests that the plastic deformation mechanism is possibly similar to what happens in the compound. Nevertheless, we cannot directly observe the dislocations in the bands by HRTEM due to technical limitation. The dislocation accommodation at grain boundaries could be relaxed during the TEM specimen thinning process,[21] and then the dislocations cannot be discerned.

The financial support of the NSF of China (50321101) is appreciated.

[1] A. S. Argon, Acta Metall. **27**, 47 (1979).
[2] M. F. Ashby and A. L. Greer, Scr. Mater. **54**, 321 (2006).
[3] B. Yang, M. L. Morrison, P. K. Liaw, R. A. Buchanan, G. Y. Wang, C. T. Liu, and M. Denda, Appl. Phys. Lett. **86**, 141904 (2005).
[4] J. J. Lewandowski and A. L. Greer, Nat. Mater. **5**, 15 (2006).
[5] C. A. Schuh, A. C. Lund, and T. G. Nieh, Acta Mater. **52**, 5879 (2004).
[6] M. W. Chen, A. Inoue, W. Zhang, and T. Sakurai, Phys. Rev. Lett. **96**, 245502 (2006).
[7] Y. F. Sun, B. C. Wei, and C. H. Shek, Appl. Phys. Lett. **87**, 051905 (2005).
[8] J. Das, M. B. Tang, K. B. Kim, R. Theissmann, F. Baier, W. H. Wang, and J. Eckert, Phys. Rev. Lett. **94**, 205501 (2005).
[9] L. Q. Xing, K. T. Ramesh, and T. C. Hufnagel, Phys. Rev. B **64**, 180201 (2001).
[10] J. Schroers and W. L. Johnson, Phys. Rev. Lett. **93**, 255506 (2004).
[11] J. M. Park and D. H. Kim, Scr. Mater. **53**, 1 (2005).
[12] H. Chen, Y. He, G. J. Shiflet, and S. J. Poon, Nature (London) **367**, 541 (1994).
[13] J. J. Kim, Y. Choi, S. Suresh, and A. S. Argon, Science **295**, 654 (2002).
[14] F. Spaepen, Nat. Mater. **5**, 7 (2006).
[15] B. Viguier, J. Bonneville, and J. L. Martin, Acta Mater. **44**, 4403 (1996).
[16] Z. F. Zhang, G. He, J. Eckert, and L. Schultz, Phys. Rev. Lett. **91**, 045505 (2003).
[17] Q. Y. Zhou, A. S. Argon, and R. E. Cohen, Polymer **42**, 613 (2001).
[18] V. G. Gryaznow and L. I. Trusov, Prog. Mater. Sci. **37**, 289 (1993).
[19] V. Yamakov and H. Gleiter, Philos. Mag. Lett. **83**, 385 (2003).
[20] K. Hajlaoui, Scr. Mater. **54**, 829 (2006).
[21] H. Van Swygenhoven, Science **296**, 66 (2002).